World Scientific
www.worldscientific.com

LARGE-SCALE FIRST PRINCIPLES CONFIGURATION INTERACTION CALCULATIONS OF OPTICAL ABSORPTION IN BORON CLUSTERS

RAVINDRA SHINDE* and ALOK SHUKLA[†]

Department of Physics
Indian Institute of Technology Bombay
Mumbai, Maharashtra 400076, India
ravindra.shinde@iitb.ac.in
[†]*shukla@phy.iitb.ac.in*

We have performed systematic large-scale all-electron correlated calculations on boron clusters $B_n(n = 2 - 5)$, to study their linear optical absorption spectra. Several possible isomers of each cluster were considered, and their geometries were optimized at the coupled-cluster singles doubles (CCSD) level of theory. Using the optimized ground-state geometries, the excited states of different clusters were computed using the multi-reference singles-doubles configuration−interaction (MRSDCI) approach, which includes electron correlation effects at a sophisticated level. These CI wave functions were used to compute the transition dipole matrix elements connecting the ground and various excited states of different clusters, eventually leading to their linear absorption spectra. The convergence of our results with respect to the basis sets, and the size of the CI expansion were carefully examined. The contribution of configurations to many body wave-function of various excited states suggests that the excitations involved are collective, plasmonic type.

Keywords: Photoabsorption; cluster; configuration interaction; boron; optical; MRSDCI.

1. Introduction

The area of cluster science has witnessed an enormous progress in terms of both the experimental and theoretical investigations of clusters of various atoms over last few decades.[1−4] Ranging from small clusters having a few atoms, to nanotubes, nanosheets, fullerenes etc., clusters have proven their usefulness in the fast emerging field of nanotechnology.[5] Because of the finiteness of the size, the properties of clusters can be greatly tuned, and, therefore they are more amenable to nanoengineering than their bulk counterpart.[6] The evolution of clusters toward the bulk with the increasing number of atoms, and the underlying mechanism, is a research topic of great contemporary interest.[7,8]

At present, boron clusters are attracting great attention because of their novel properties and potential applications in nanotechnology and hydrogen storage−related capabilities.[9−12] Boron atom, having s^2p^1 valence electronic configuration, has short covalent radius and tends to form strong directional bonds producing clusters of covalent nature. Because of this strong covalent bonding, its

hardness is close to that of diamond. The ability of boron to form structures of any size due to catenation is only comparable to its neighbor carbon.[9] Planar boron clusters exhibit aromaticity[13] due to the presence of itinerant π electrons, and some of them are analogous to aromatic hydrocarbons.[14] Boron fullerenes, boron sheets and single-sheet boron nitride — a graphene analog — are the other examples of boron-based clusters.

As far as the studies of boron-based clusters are concerned, small ionic boron clusters $B_n^+ (n \leq 20)$ were experimentally studied by Hanley, Whitten and Anderson.[15] Wang and coworkers have reported joint theoretical and experimental studies of the electronic structure of bare boron wheels, rings, tubes and large quasi-planar clusters.[14,16−18] Using the photoelectron spectroscopy, they predicted that tubular B_{20} can act as the smallest boron single-walled nanotube. Transition metal−centered boron ionic ring clusters were studied by Constantin *et al.*[17] in a photoelectron spectroscopy experiment, supported by first-principles calculations. The abundance spectrum of boron clusters generated by laser ablation of hexagonal boron nitride was studied by time-of-flight measurements performed by La Placa, Roland and Wynne.[19] They also postulated the existence of $B_{36}N_{24}$ cluster having a structure similar to that of C_{60} fullerene. Lauret *et al.*[20] probed the optical transitions in single-walled boron nitride nanotubes by means of optical absorption spectroscopy.

Larger pure boron clusters have also been investigated extensively. Cage-like structure of B_{80} — similar to C_{60} fullerene — has been proposed theoretically.[21] A density functional theory (DFT) study of pure boron sheets and nanotubes was carried out by Cabria, Lopez and Alonso to explore their potential hydrogen storage materials.[11] Chacko, Kanhere and Boustani investigated different equilibrium geometries of B_{24} cluster using Born−Oppenheimer molecular dynamics within the framework of DFT.[22] Abdurahman *et al.*[23] studied the ladder-like planar boron chains B_n ($n = 4−14$), and computed their static dipole polarizabilities using the *ab initio* CI method. Johansson discussed strong toroidal ring currents in B_{20} and other toroidal boron clusters.[24] Double aromaticity was proposed in toroidal boron clusters B_{2n} ($n = 6, 14$) by Bean and Fowler.[25]

Regarding the smaller-sized boron clusters, an early theoretical study of boron dimer was carried

out by Langhoff and Bauschlicher,[26] who performed extensive calculations using the complete-active-space self-consistent-field (CASSCF) multireference configuration interaction (MRCI) with a large basis set. A similar study was carried out by Bruna and Wright[27] for the excited states of B_2, and by Howard and Ray[28] using the many-body perturbation theory. A systematic geometry and electronic structure calculations of bare boron clusters was reported by Boustani.[29] He performed all-electron calculations at the SDCI level, but the contracted Gaussian basis sets used were small. Niu, Rao and Jena,[30] using DFT and quantum chemical methods, presented an account of electronic structures of neutral and charged boron clusters. In their study on small clusters, Möller−Plesset perturbation theory of fourth order (MP4) was used to account for the electron correlation effects. More recently, Atiş, Özdogan and Güvenç investigated structure and energetics of boron clusters using the DFT.[31] Aromaticity in planar boron clusters was addressed by Aihara, Kanno and Ishida.[32]

In spite of many theoretical studies of boron clusters of various shapes and sizes, very little experimental information about their ground and excited states is available. Conventional mass spectrometry can distinguish between different clusters only according to their mass but not according to their geometry. One has to rely on other theoretical or experimental data to be able to differentiate one isomer from another. For example, using first-principles calculations of vibrionic fine structure in C_{20}^-, and comparing it with experimentally available data, Saito and Miyamoto[33] identified the cage and bowl structures. Optical absorption spectroscopy, coupled with extensive theoretical calculations of the optical absorption spectra, can be used to distinguish between distinct isomers of clusters produced experimentally, because normally optical absorption spectra are sensitive to the geometries of the clusters. The optical absorption of alkali metal clusters has been extensively studied both experimentally and theoretically.[34−38] However, very few such studies exist for the case of boron clusters. Marques and Botti[39] calculated optical absorption on different B_{20} isomers using time-dependent (TD) DFT. Boron fullerenes such as B_{38}, B_{44}, B_{80} and B_{92} were also studied by Botti and coworkers[40] using the same technique. However, to the best of out knowledge, there are no experimental and theoretical studies of

optical absorption on other bare boron clusters, particularly the smaller ones. It is with the aim of filling this void that we undertake a systematic study of the optical absorption in small boron clusters B_n ($n = 2 - 5$), employing the MRSDCI method, and high-quality Gaussian basis functions. We perform careful geometry optimization for each possible isomer and compute the optical absorption spectra of various structures. We also analyze the many-body wave functions of various excited states contributing to the peaks in the computed spectra, and conclude that most of the excitations are collective in nature, signaling the presence of plasmons.

The remainder of this paper is organized as follows. Section 2 describes the theoretical and computational details of the work, followed by Sec. 3, in which our results are presented and discussed. In Sec. 4, we present our conclusions and discuss possibilities for future work. Detailed information about various excited states contributing to optical absorption is presented in the Appendix.

2. Theoretical and Computational Details

The geometry optimization of various isomers was done using the size-consistent coupled-cluster singles doubles (CCSD)−based analytical gradient approach, as implemented in the package GAMESS-US.[41] For

the purpose, we used the 6-311G(d,p) basis set included in the program library,[41] which is known to be well suited for this task. The process of optimization was initiated by using the geometries reported by Atiş *et al.*,[31] based upon first-principles DFT-based calculations. For some simple geometries such as B_2, B_3 (D_{3h} symmetry), the optimization was carried out manually, by performing the MRSDCI calculations at different geometries, and locating the energy minima. Figure 1 shows the final optimized geometries of the isomers studied in this paper.

Once the ground state geometries of various isomers were determined, the correlated calculations were performed to calculate their low-lying excited states using the multi-reference singles-doubles configuration-interaction (MRSDCI) approach as implemented in the computer program MELD.[42] MRSDCI approach is a well-established quantum-chemical approach in which one considers singly and doubly excited configurations from a number of reference configurations, leading to a good treatment of electron correlations, both for the ground and the excited states, in the same calculation. Using the ground- and excited-state wave functions obtained from the MRSDCI calculations, electric dipole matrix elements are computed and subsequently utilized to compute the linear absorption spectrum assuming a Lorentzian line shape. By analyzing the wave functions of the excited states

(a) B_2, $D_{\infty h}$, $^3\Sigma_g^-$ (b) B_3, D_{3h}, $^2A_1'$ (c) B_3, $D_{\infty h}$, $^2\Sigma_g^-$ (d) B_4, D_{2h}, ^1A_g (e) B_4, D_{4h}, $^1A_{1g}$

(f) B_4, $D_{\infty h}$, $^1\Sigma_g^-$ (g) B_4, C_{2v}, $^1A_1$ (h) B_5, C_{2v}, $^2B_2$ (i) B_5, C_s, ^2A
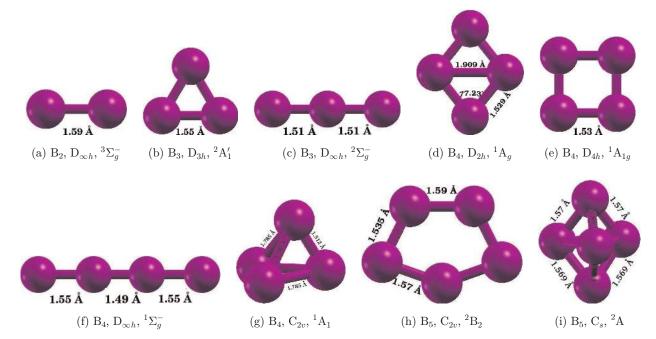
Fig. 1. Geometry optimized structures of boron clusters with point group symmetry and the electronic ground state at the configuration interaction level (color online).

contributing to the peaks of the computed spectrum obtained from a given calculation, bigger MRSDCI calculations were performed by including a larger number of reference states. The choice of the reference states to be included in a given calculation was based upon the magnitude of the corresponding coefficients in the CI wave function of the excited state (or states) contributing to a peak in the spectrum. This procedure was repeated until the computed spectrum converged within an acceptable tolerance, and all the configurations contributing significantly to various excited states were included in the list of the reference states. In the past, we have used such an iterative MRSDCI approach on a number of conjugated polymers to perform large-scale correlated calculations of their linear and non-linear optical properties.[43−46]

The number of molecular orbitals, and thus the size of the CI expansion, increases rapidly with the increasing number of atoms in the clusters. Such a proliferation in the size of calculations can essentially make high-quality MRSDCI calculations impossible even for clusters of the sizes discussed in this work. Therefore, wherever possible, we have used the point-group symmetries corresponding to D_{2h}, and its subgroups, at all levels of calculations to reduce the size of the CI expansions. During the MRSDCI calculations, the frozen-core approximation was employed, i.e., while constructing the CI expansion, no virtual excitations from the $1s$ core electrons of the boron atoms of the cluster were considered. Similarly, excitations into very high energy virtual orbitals were not considered with the purpose of keeping the calculations manageable. The impact of both the frozen-core approximation, and the deletion of high-energy virtual orbitals, along with the influence of the choice of the basis sets on our calculations will be examined carefully in the next section.

3. Results and Discussion

In this section, first we discuss the convergence of our calculations with respect to various approximations and truncation schemes. Thereafter, we present and discuss the results of our calculations for various clusters.

3.1. *Convergence of calculations*

Here, we carefully examine the convergence of the calculated absorption spectra with respect to the size and quality of the basis set, along with various truncation schemes in the CI calculations.

3.1.1. *Choice of the basis set*

In general, the results of electronic structure calculations depend upon the quality and the size of the basis set employed. While several contracted Gaussian basis functions have been devised which can deliver high-quality results on various quantities such as the total energy, correlation energy, and the static polarizabilities of molecules, to the best of our knowledge the basis set dependence of linear optical absorption has not been explored. Since boron shows strong covalent bondings, the basis set used for calculations should have diffuse Gaussian contractions. Therefore, to explore the basis set dependence of computed spectra, we used several basis sets[47,48] to compute the optical absorption spectrum of the smallest cluster, i.e., B_2. For the purpose, we used correlation-consistent basis sets named AUG-CC-PVTZ, DAUG-CC-PVDZ, AUG-CC-PVDZ, CC-PVDZ, and DZP, which consist of polarization functions along with diffuse exponents, and were designed specifically for post Hartree−Fock correlation calculations.[47,48] From the calculated spectra presented in Fig. 2, the following trends emerge: the spectra computed by various augmented basis sets (AUG-CC-PVTZ, DAUG-CC-PVDZ, AUG-CC-PVDZ) are in good agreement with each other in the energy range up to 8 eV, while those obtained using the nonaugmented sets (CC-PVDZ and DZP) disagree with them
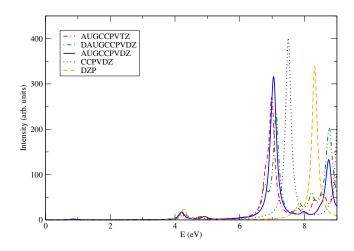

Fig. 2. Optical absorption in B_2 calculated using various Gaussian contracted basis sets. Increasing more and more diffuse d-type Gaussians shows negligible effect on optical spectra (color online).

substantially, particularly in the higher energy range. Given the fact that augmented basis sets are considered superior for molecular calculations, we decided to perform calculations on the all the clusters using the AUG-CC-PVDZ basis set. This is the smallest of the augmented basis sets considered by us, and, therefore, does not cause excessive computational burden when used for larger clusters.

3.1.2. *Orbital truncation schemes*

If the total number of orbitals used in a CI expansion is N, the number of configurations in the calculation proliferates as $\approx N^6$, which can become intractable for large values of N. Therefore, it is very important to reduce the number of orbitals used in the CI calculations. The occupied orbitals are reduced by employing the so-called "frozen-core approximation" described earlier, while the unoccupied (virtual) set is reduced by removing very high-energy orbitals.

The influence of freezing the $1s$ core orbitals on the optical absorption spectrum of B_2 cluster is displayed in Fig. 3, from which it is obvious that it makes virtually no difference to the results whether or not the core orbitals are frozen. The effect of removing the high-energy virtual orbitals on the absorption spectrum of B_2 is examined in Fig. 4. From the figure it is obvious that if all the orbitals above the energy of 1 Hartree are removed, the absorption spectrum stays unaffected. Therefore, in rest of the calculations, wherever needed, orbitals above this energy cutoff were removed from the list of
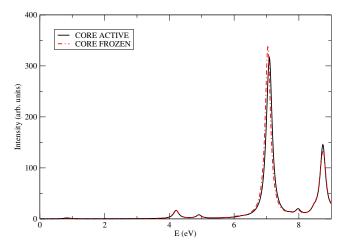

Fig. 4. The effect of the number of active orbitals (N_{act}) on the optical absorption spectrum of B_2. Until $N_{act} = 42$, the optical spectrum does not exhibit any significant change. It corresponds to a cutoff of 1.0 Hartree (≈ 27.2 eV) virtual orbital energy (color online).

active orbitals. Theoretically speaking, this cutoff is sound, because we are looking for absorption features in the energy range much smaller than 1 Hartree.

3.1.3. *Size of the CI expansion*

As mentioned earlier, the electron correlation effects in both the ground and the excited states were accounted in our calculations by including the relevant configurations in the reference list of the MRSDCI expansion. The greater numerical accuracy demands the inclusion of a large number of configurations in the reference list, but that leads to a rapid growth in the size of the CI expansion, making the calculations numerically prohibitive. However, here we are interested in computing the energy differences rather than the absolute energies of various states, for which good accuracy can be achieved even with moderately large CI expansions. In Table 1, we present the average number of reference states (N_{ref}) included in the MRSDCI expansion and average number of configurations (N_{total}) for different isomers. For a given isomer, the average has been calculated across different irreducible representations which were needed in these symmetry adapted calculations in order to compute the ground and various excited states. The extensiveness of our calculations can be seen from the number N_{total}, which is $\approx 77\,000$ for the simplest cluster, and around four million for each symmetry subspace of B_5. This makes us believe that our results are fairly accurate.

Fig. 3. The effect of freezing the core orbitals ($1s$) of boron atoms on optical absorption spectrum of B_2. It renders almost no effect on optical absorption spectrum (color online).
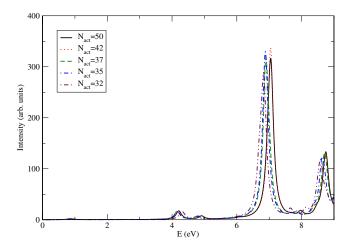
Table 1. The average number of reference configurations (N_{ref}), and average number of total configurations (N_{total}) involved in MRSDCI calculations of various isomers of boron clusters.

Cluster	Isomer	N_{ref}	N_{total}
B_2	Linear	24	77 245
B_3	Triangular	36	596 798
	Linear	41	671 334
B_4	Rhombus	37	1 127 918
	Square	40	1 070 380
	Linear	34	1 232 803
	Distorted Tetrahedron	28	1 253 346
B_5	Pentagon	22	3 936 612
	Distorted Tri. bipyramid[a]	7	3 927 508

Note: [a]C_s symmetry of isomer converted to C_1 in calculations.

Before we discuss the absorption spectrum for each isomer, we present the ground state energies along with the relative energies of each isomer given in Table 2. The MRSDCI energy convergence threshold was 10^{-5} for all the isomers, with 10^{-4} as convergence threshold for configuration coefficients. From the results it is obvious that as far as the energetics are concerned, for the B_3 the triangular structure is most stable, while for B_4 and B_5 the rhombus and pentagonal structures, respectively, are favorable.

3.2. Calculated photoabsorption spectra of various clusters

Next we present and discuss the results of our photoabsorption calculations for each isomer.

Table 2. Ground state (GS) energies (in Hartree) at MRSDCI level and the relative energies (in eV) of different isomers of clusters.

Cluster	Isomer	GS energy (Ha)	Relative energy (eV)
B_2	Linear	−49.27844	0.00
B_3	Triangular	−73.98998	0.00
	Linear	−73.92906	1.66
B_4	Rhombus	−98.74004	0.00
	Square	−98.73785	0.06
	Linear	−98.66575	2.02
	Distorted Tetrahedron	−98.63213	2.94
B_5	Pentagon	−123.42652	0.00
	Distorted Tri. Bipyramid	−123.31485	3.04

3.2.1. B_2

The simplest and most widely studied cluster of boron is B_2 with $D_{\infty h}$ point group symmetry. Using the SDCI method, we obtained its optimized bond length to be 1.59 Å (*cf.* Fig. 1(a)), which is in excellent agreement with the experimental value 1.589 Å.[49] Using a DFT-based methodology, Atiş *et al.*[31] obtained a bond length of 1.571 Å, while Howard and Ray calculated it to be 1.61 Å, using the fourth-order perturbation theory (MP4).[28]

Because the ground state of B_2 is a spin triplet, its many-particle wave function predominantly consists of a configuration with two degenerate singly-occupied molecular orbitals (SOMO) referred to as H_1 and H_2 in the rest of the discussion. The excited state wave functions will naturally consist of configurations involving electronic excitations from the occupied MOs to the unoccupied MOs starting from lowest unoccupied molecular orbital (LUMOs, L for short). Our calculated photoabsorption spectrum shown in Fig. 5 is characterized by weaker absorptions at low energies, and a very intense one at high energy. The many-particle wave functions of excited states contributing to various peaks are presented in Table A1. A feeble peak appears near 0.85 eV, dominated by $H_2 \rightarrow L$ and $H_2 \rightarrow L+4$ excitations compared to the HF reference configuration. It is followed by a couple of smaller peaks at 4.20 eV and 4.91 eV. The most intense peak is found at 7.05 eV, to which two closely spaced states
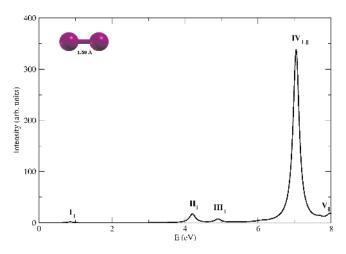

Fig. 5. The linear optical absorption spectrum of B_2, calculated using the MRSDCI approach. The peaks corresponding to the light polarized along the molecular axis are labeled with the subscript $\parallel$, while those polarized perpendicular to it are denoted by the subscript $\perp$. For plotting the spectrum, a uniform linewidth of 0.1 eV was used.

contribute. Transition to the state near 6.97 eV is polarized transverse to the bond length, while the one close to 7.05 eV carries the bulk of oscillator strength, and is reached by longitudinally polarized photons. All these states exhibit strong mixing of singly-excited configurations. Near 8 eV, a smaller peak appears which has strong contributions from doubly-excited configurations $H - 1 \rightarrow L$; $H_1 \rightarrow L + 2$ and $H - 1 \rightarrow L$; $H_2 \rightarrow L + 2$. The wave functions of the excited states contributing to all the peaks exhibit strong configuration mixing, instead of being dominated by single configurations, pointing to the plasmonic nature of the optical excitations.[50]

3.2.2. B_3

Boron trimer has two possible isomers, triangular and the linear one shown in Figs. 1(b) and 1(c). We found equilateral triangle with D_{3h} symmetry to be the most stable isomer. The optimized bond length for triangular isomer is 1.55 Å, with the ground state $(^2A_1')$ energy 1.66 eV lower than that of its linear counterpart. We also explored the possibility of isosceles triangular structure as a favorable one, because B_3 is an open-shell system, making it a possible candidate for Jann−Teller distortion. However, the CCSD optimized geometry corresponding to the isosceles structure is slightly different compared to the equilateral one, so it is unlikely to affect the optical absorption spectrum in a significant manner. Our calculated bond length is in good agreement with experimental value 1.57 Å,[15] as well as with other reported theoretical values of 1.553 Å,[29] 1.56 Å[28] and 1.548 Å.[31]

The linear B_3 isomer with the $D_{\infty h}$ symmetry, and the $^2\Sigma_g^-$ as ground state, was found to have equal bond lengths. Our SDCI optimized bond length of 1.51 Å agrees well with the value 1.518 Å reported by Atiş *et al.*[31]

The photoabsorption spectra of two isomers of B_3 are presented in Figs. 6 and 7. The corresponding many-particle wave functions of excited states contributing to various peaks are presented in Table A2 and A3. It is obvious that in the linear structure, absorption begins at around the same energy as in the triangular one. In the triangular isomer on the other hand, most of the intensity is concentrated at rather high energies, except for a weaker peak close to 3 eV. The optical spectra of linear isomer begin with very weak peaks at 0.7 eV (longitudinal polarization) and 2.7 eV (transverse
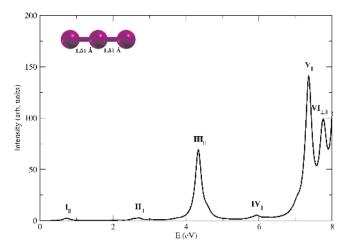

Fig. 6. The linear optical absorption spectrum of linear B_3, calculated using the MRSDCI approach. The peaks corresponding to the light polarized along the molecular axis are labeled with subscript ∥, while those polarized perpendicular to it are denoted by the subscript ⊥. For plotting the spectrum, a uniform linewidth of 0.1 eV was used.

polarization), with their many-particle wave functions dominated by singly-excited configurations. The relatively intense peak at 4.3 eV corresponding to a longitudinally polarized transition, is dominated by doubly-excited configurations. It is followed by a small peak mainly due to single excitation $H - 2 \rightarrow L$, near 5.9 eV. The most intense peak of the spectrum occurs at 7.4 eV, followed by another strong peak close to 7.7 eV. Both
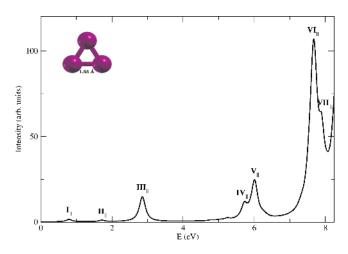

Fig. 7. The linear optical absorption spectrum of triangular B_3 calculated using the MRSDCI approach. Peaks corresponding to light polarized in the plane of the molecule are labeled with subscript ∥, while those polarized perpendicular to the plane are denoted by the subscript ⊥. For plotting the spectrum, a uniform linewidth of 0.1 eV was used (color online).

the features correspond to longitudinally polarized transitions, with the many-particle wave functions of the concerned states being strong mixtures of single and double excitations with respect to the HF reference state. We note that in the absorption spectrum of the linear cluster, quite expectedly, the bulk of the oscillator strength is carried by longitudinally polarized transitions.

Because the triangular cluster is a planar cluster, its orbitals can be classified as in-plane σ orbitals, and the out-of-plane π orbitals. Both the HOMO (a singly occupied orbital, in this case) and the LUMO for this isomer are σ-type orbitals. For this system, two types of optical absorptions are possible: (a) those polarized in the plane of the cluster, and (b) the ones polarized perpendicular to that plane. Our calculations reveal that the transitions corresponding to perpendicular polarization (z direction), except for a couple of peaks, have negligible intensities. From Fig. 7 it is obvious that the optical absorption in the triangular isomer starts with a very weak z-polarized feature near 0.8 eV (peak I), corresponding to a state with the wave function dominated by single excitations ($\pi \rightarrow \sigma^*$). This is followed by a series of peaks ranging from II to VI which correspond to the photons polarized in the plane of the cluster. All these peaks are dominated by states consisting primarily of singly-excited configurations of the $\sigma \rightarrow \sigma^*$ type. The most intense peak VI is followed by a shoulder-like feature (VII) corresponding to a z-polarized absorption.

If we compare the absorption spectra of the linear and the triangular B$_3$, the peak at 4.34 eV in the spectrum of the linear cluster is the distinguishing feature, and can be used to differentiate between the two isomers.

3.2.3. B_4

For the B$_4$ cluster, we investigated the rhombus, square, linear and tetrahedral structures. While the rhombus-shaped isomer was found to have the lowest energy, the square isomer is higher in energy only by a small amount. As a matter of fact, at the HF level the energies of the two isomers were found to be almost degenerate. It was only after the electron correlation effects were included at the CI level that the rhombus stabilized by ≈ 0.06 eV (*cf.* Table 2) with respect to the square. For the rhombus, the ground state was ^1A_g, with the optimized bond length 1.529 Å, and the short diagonal length

1.909 Å. These results are in good agreement with with the corresponding lengths of 1.528 Å and 1.885 Å reported by Boustani,[29] and 1.523 Å and 1.884 Å computed by Atiş *et al.*[31] Both HOMO and LUMO of rhombus isomer are σ orbitals.

For the square isomer, with D$_{4h}$ symmetry, the electronic ground state is expectedly $^1A_{1g}$. As shown in Fig. 1(e), our optimized bond length is 1.53 Å, which agrees well with the values 1.527 Å and 1.518 Å as reported in Refs. 29 and 31. In this isomer, HOMO is a σ orbital while LUMO is a π orbital.

Linear B$_4$, with the D$_{\infty h}$ symmetry, has the electronic ground state of $^1\Sigma_g^-$. However, the energetically linear structure is 2.02 eV higher than the rhombus one (*cf.* Table 2) which rules out its existence at the room temperatures. As per Fig. 1(f), the central bond length was found to be 1.49 Å, with the two outer bonds being 1.55 Å in length. For the same bonds, Atiş *et al.* reported these lengths to be 1.487 Å and 1.568 Å, respectively.[31]

The distorted tetrahedral structure having C$_{3v}$ symmetry, made up of four isosceles triangular faces with lengths 1.785 Å, 1.785 Å and 1.512 Å. This isomer also lies much higher in energy as compared to the most stable rhombus structure.

The absorption spectra of rhombus, square, linear, and tetrahedral isomers are presented in Figs. 8, 9, 10, and 11, respectively. From the figures, it is obvious that the general features of the absorption
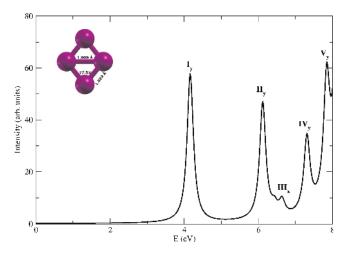

Fig. 8. The linear optical absorption spectrum of B$_4$ rhombus geometry using the MRSDCI approach. Isomer is aligned in $x - y$ plane with short diagonal along x-axis. Peaks corresponding to light polarized along x and y-axis are labeled with subscript x and y. For plotting the spectrum, a uniform linewidth of 0.1 eV was used (color online).
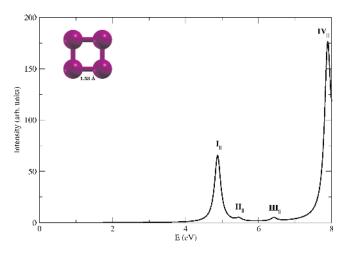
Fig. 9. The linear optical absorption spectrum of B_4 square geometry using MRSDCI approach. Isomer is aligned in $x-y$ plane. Spectrum represents the equal contribution from light polarized in x and y direction. Peaks corresponding to light polarized in the plane of the molecule are labeled with subscript $\parallel$. For plotting the spectrum, a uniform linewidth of 0.1 eV was used (color online).

Fig. 11. The linear optical absorption spectrum of B_4 distorted tetrahedral geometry using the MRSDCI approach. Peaks corresponding to light polarized along x-, y- and z-axis are labeled with subscript x, y and z, respectively. For plotting the spectrum, a uniform linewidth of 0.1 eV was used (color online).

spectra of rhombus and square isomers are similar, except that the rhombus spectrum, with the onset of the absorption near 4 eV, is blue-shifted by about 1 eV as compared to the square. The absorption spectrum of the linear structure is slightly red-shifted as compared to the rhombus and square-shaped isomers, with the majority of absorption occurring in the energy range 5–8 eV.
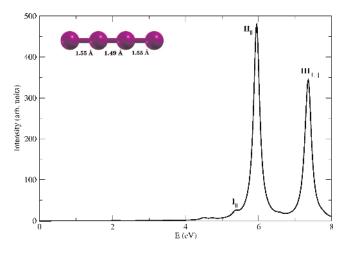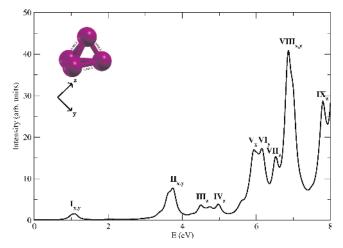

Fig. 10. The optical absorption spectrum of linear B_4, calculated using the MRSDCI approach. The peaks corresponding to the light polarized along the molecular axis are labeled with subscript $\parallel$, while those polarized perpendicular to it are denoted by the subscript $\perp$. For plotting the spectrum, a uniform linewidth of 0.1 eV was used.

Since B_4 rhombus isomer has D_{2h} symmetry, we can represent the absorption due to light polarized in different directions in terms of irreducible representations of D_{2h}. So absorption due to in-plane polarized light corresponds to B_{1u} and B_{2u}, while B_{3u} corresponds to light polarized in the direction perpendicular to the plane of the isomer.

The polarization resolved absorption spectrum of rhombus B_4, as shown in Fig. 8, exhibits a rather blue-shifted nature as compared to the linear isomer. The many-particle wave functions of excited states contributing to various peaks are presented in Table A4. The onset of spectrum is seen at 4.15 eV followed by a peak at around 6.12 eV. Both of them are due to y-polarized component, i.e., along the larger diagonal. The dominant contribution to these peaks come from $\sigma \rightarrow \pi^*$ for former, and $\pi \rightarrow \pi^*$ for latter. The x-component does not contribute much in the whole spectrum, except for minor peaks at 4.2 eV and 6.6 eV. It is characterized by mainly $\pi \rightarrow \pi^*$ type transitions. It is followed by a relatively low intensity peak at 7.3 eV due to y-polarized component with leading contribution from $\sigma \rightarrow \pi^*$ transitions. The most intense peak, at 7.84 eV, having y-polarization component, is characterized by $\sigma \rightarrow \pi^*$ type of transitions. There are no direct $H \rightarrow L$ transitions for this isomer, because they are dipole forbidden. The absorption due to light polarized in the direction perpendicular to the plane of isomer is negligible.

The square B_4 isomer, because of its symmetry, gets equal contribution to absorption spectrum from both x- and y-component. It corresponds to in-plane polarization due to B_{1u} and B_{2u} irreducible representation, while B_{3u} corresponds to light polarized in the direction perpendicular to the plane of the isomer. However, in this isomer also, the contribution due to latter is quite negligible. The many-particle wave functions of excited states contributing to various peaks are presented in Table A5. It shows just one major peak at $4.88\,\mathrm{eV}$ below $7\,\mathrm{eV}$, characterized by $\sigma \to \pi^*$; $\sigma \to \pi^*$ double excitation. Two smaller peaks appear in this range at $5.5\,\mathrm{eV}$ and $6.4\,\mathrm{eV}$, with leading contributions from $\sigma \to \pi^*$; $\sigma \to \pi^*$ and $\sigma \to \pi^*$; $\pi \to \pi^*$ excitations, respectively. Beyond $7\,\mathrm{eV}$, there are many closely spaced peaks, including the most intense one at $7.89\,\mathrm{eV}$. It is characterized by double excitation $\sigma \to \pi^*$; $\pi \to \pi^*$. In this isomer also, a direct $H \to L$ transitioin is forbidden. Though, there is very little difference in total energies of rhombus and square isomers of B_4, their optical absorption spectra are completely different. They can be easily identified from each other by looking at the number of peaks below $7\,\mathrm{eV}$ energy. Rhombus exhibits two major peaks, while square has just one.

Linear B_4 isomer exhibits absorption with few, but sharp peaks. The many-particle wave functions of excited states contributing to various peaks are presented in Table A6. The onset of optical absorption occurs near $4.5\,\mathrm{eV}$, due to absorption of long-axis polarized light, followed by two major peaks at $5.95\,\mathrm{eV}$ and $7.36\,\mathrm{eV}$. The first of these two intense peaks, peak II is dominated by singly-excited configurations, while the second one (peak III) is a strong mixture of both singly- and doubly-excited configurations with respect to the HF reference configuration.

The 3D structure, a distorted tetrahedral isomer, exhibits an absorption spectrum very different from other isomers, as displayed in Fig. 11. The many-particle wave functions of excited states contributing to various peaks are presented in Table A7. It is the only B_4 isomer to exhibit peaks below $4\,\mathrm{eV}$. The absorption spectrum is spread over a much larger energy range, and is almost continuous. The oscillator strengths associated with various peaks are much smaller than in other isomers, and most of the peaks appear pairwise. The onset of absorption spectrum is seen at around $1.1\,\mathrm{eV}$, characterized mainly by an excited state dominated by single-excitation $H \to L$ (*cf.* Table A7). In this isomer, in contrast to other B_4 isomers, direct $H \to L$ transitions are allowed. Higher energy peaks in this isomer are dominated by doubly-excited configurations, and, are, therefore, sensitive to the electron-correlation effects.

3.2.4. B_5

We investigated two isomers of B_5: (a) Jahn−Teller distorted pentagon with the C_{2v} symmetry, and (b) a triangular bipyramid with the C_s point group symmetry. The latter one is the second 3D structure of the boron clusters probed in this work. The lowest lying pentagon isomer, has $^2B_2$ electronic ground state, and is $3.04\,\mathrm{eV}$ lower in energy as compared to the bipyramid structure. For the pentagon, the symmetry of ground state at the SCF level was A_1, however, at the MRSDCI level the B_2 state became lower in energy, in agreement with the previous calculations of Boustani.[29] Our optimized geometry for the pentagon (Fig. 1(h)) corresponds to an average bond length of $1.56\,\text{Å}$, as against $1.57\,\text{Å}$ reported by Boustani,[29] and $1.644\,\text{Å}$ reported by Atiş *et al.*[31] The singly-occupied molecular orbital (denoted by H) and LUMO of pentagon isomers are of π and σ type, respectively. The bond lengths for the bipyramid structure are shown in Fig. 1(i), with an average bond length of $1.704\,\text{Å}$. The triangular base was found to be isosceles with $1.97\,\text{Å}$ as equal sides, and $1.75\,\text{Å}$ as the other side.

The absorption spectra of the two isomers are presented in Figs. 12 and 13. The many-particle wave functions of excited states contributing to various peaks are presented in Tables A8 and A9, respectively. From the figures it is obvious that the absorption in the bipyramid starts at much lower energies as compared to the pentagonal isomer. Intense absorption peaks in pentagon B_5 are located at energies higher than $5\,\mathrm{eV}$, with three equally intense peaks at $5.58\,\mathrm{eV}$, $6.30\,\mathrm{eV}$ and $7.16\,\mathrm{eV}$, with the photons polarized along the plane of the molecule direction. It has an underlying low intensity absorption contribution from photons polarized along z-direction, which is perpendicular to the molecular plane. The major contribution to the peak at $5.58\,\mathrm{eV}$ comes from $\pi \to \sigma^*$ and $\sigma \to \sigma^*$, single excitations. The latter configuration also contributes to the most intense peak at $6.30\,\mathrm{eV}$. The peak at $7.16\,\mathrm{eV}$ is mainly due to $\sigma \to \sigma^*$ type transitions.
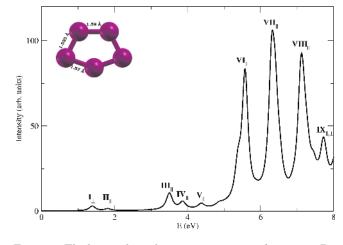
Fig. 12. The linear photoabsorption spectrum of pentagon B_5, calculated using the MRSDCI approach. The peaks corresponding to the light polarized in the plane of the molecule are labeled with subscript $\parallel$, while those polarized perpendicular to it are denoted by the subscript $\perp$. For plotting the spectrum, a uniform linewidth of 0.1 eV was used (color online).

Since the B_5 triagonal bipyramid isomer is not a symmetric one, the calculations were done using C_1 symmetry, thereby increasing the difficulty in diagonalizing the Hamiltonian. Hence, in order to reduce the matrix size, we have used a smaller number of reference configurations, and also relaxed the energy convergence threshold criterion a little.

The optical absorption spectrum of B_5 triangular bipyramid isomer is exhibited by almost equally
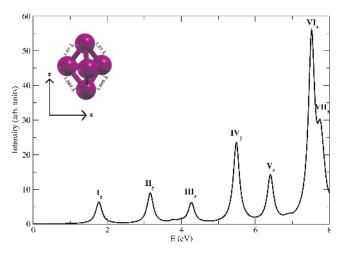

Fig. 13. The linear photo-absorption spectrum of distorted triangular bipyramid B_5, calculated using the MRSDCI approach. Peaks corresponding to light polarized along x, y and z-axis are labeled with subscript x, y and z, respectively. For plotting the spectrum, a uniform linewidth of 0.1 eV was used (color online).

spaced peaks at relatively lower energies. The optical absorption starts at 1.74 eV characterized by $H - 1 \rightarrow L + 4$ configuration. It is followed by two equal intensity peaks at 3.16 eV and 4.27 eV with contributions from single excitations $H - 2 \rightarrow H$ and $H - 1 \rightarrow L + 2$, respectively. The most intense peak is found at 7.52 eV dominated by the doubly excited configuration $H - 2 \rightarrow H$; $H - 1 \rightarrow L + 2$. There are two distinguishing features as far as the optical absorption in the two isomers is concerned: (a) presence of three intense peaks in the higher energy region of the absorption spectrum of the pentagonal isomer, and (b) occurrence of equally spaced absorption peaks at lower energies in the spectrum of bipyramidal isomer.

4. Conclusions and Outlook

We presented systematic large-scale all-electron correlated calculations of photoabsorption spectra of boron clusters B_n, $(n = 2 - 5)$ with several possible isomers of each cluster. The calculations were performed using the MRSDCI method, which takes electron correlations into account at a sophisticated level, both for the ground and the excited states. For a cluster consisting of a given number of atoms, significant changes were observed in absorption spectra for different isomers, indicating a strong structure−property relationship. Therefore, our computed spectra can be used in the future photoabsorption experiments to distinguish between different isomers of a cluster, something which is not possible with the conventional mass spectrometry. We also analyzed the many-particle wave functions of various excited states and found them to be a mixture of a large number of configurations, indicating the nature of photoexcited states in these clusters to be plasmonic.[49] A noteworthy aspect of the groundstate photoabsorption of various clusters was the absence of high-intensity peaks in the low-energy region of the spectrum. The most intense peaks occurred at higher energies involving orbitals away from the Fermi level, consistent with the fact that the bulk boron is an indirect bandgap semiconductor, with no optical absorption at the gap. In other words, optical absorption features of bulk boron were already evident in smaller clusters. Given the fact that aluminum has the same valence shell structure as boron, it will be interesting to perform a similar set of calculations on small aluminum clusters, in order to compare

and contrast their photophysics. Calculations along those directions are presently underway in our group, and results will be communicated in future publications.

Acknowledgments

Appendix: Excited State CI Wavefunctions, Energies and Transition Moments

In the Tables A1−A9 we have given the excitation energies (with respect to the ground state), the many body wavefunction and the oscillator strengths of the excited states corresponding to the peaks in the photoabsorption spectra of various isomers listed in Fig. 1, and discussed in Sec. 3.

Table A1. Excitation energies, E, and many-particle wave functions of excited states corresponding to the peaks in the linear absorption spectrum of B_2 (*cf.* Fig. 5), along with the oscillator strength of the transitions ($f_{12} = \frac{2}{3}\frac{m_e}{\hbar^2}(E_2 - E_1)\sum_i |\langle m|d_i|G\rangle|^2$), where, $|m\rangle$ denotes the excited state in question, $|G\rangle$, the ground state, and d_i is the ith Cartesian component of the electric dipole operator.

Peak	E (eV)	f_{12}	Polarization	Wave Function
GS[a]				$|\text{HF}\rangle$ (0.8673)
				$|H-1 \to L; H-1 \to L\rangle$ (0.2706)
				$|H-1 \to L; H-1 \to L+4\rangle$ (0.1283)
I	0.845	0.0156	transverse	$|H_2 \to L\rangle$ (0.8742)
				$|H_2 \to L+4\rangle$ (0.2194)
II	4.207	0.1463	longitudinal	$|H-1 \to L\rangle$ (0.7599)
				$|H_1 \to L+7\rangle$ (0.2873)
				$|H_2 \to L+7\rangle$ (0.2873)
III	4.914	0.0558	transverse	$|H-1 \to L; H-1 \to L+2\rangle$ (0.7553)
				$|H-2 \to L+2\rangle$ (0.3186)
				$|H-1 \to L+7\rangle$ (0.266)
IV	6.97	0.5651	transverse	$|H_2 \to L+4\rangle$ (0.5600)
				$|H_2 \to L+5\rangle$ (0.5150)
	7.05	2.3743	longitudinal	$|H-1 \to L\rangle$ (0.4462)
				$|H_2 \to L+3\rangle$ (0.3346)
				$|H_1 \to L+3\rangle$ (0.3346)
				$|H-1 \to L+4\rangle$ (0.2921)
V	7.973	0.0906	longitudinal	$|H-1 \to L; H_2 \to L+2\rangle$ (0.5613)
				$|H-1 \to L; H_1 \to L+2\rangle$ (0.5613)
				$|H-1 \to L+4\rangle$ (0.2303)

[a]GS does not correspond to any peak, instead it corresponds to the ground state wavefunction of the isomer.

Note: Longitudinal and transverse polarization corresponds to the absorption due to light polarized along and perpendicular to the molecular axis, respectively. In the wave function, the bracketed numbers are the CI coefficients of a given electronic configuration. Symbols H_1, H_2 denote SOMOs discussed earlier, and H, and L, denote HOMO and LUMO orbitals, respectively. HF denotes the Hartree−Fock configuration.

Table A2. Excitation energies, E, and many-particle wave functions of excited states corresponding to the peaks in the linear absorption spectrum of triangular B_3 (*cf.* Fig. 7), along with oscillator strength of transition ($f_{12} = \frac{2}{3}\frac{m_e}{\hbar^2}(E_2 - E_1)\sum_i |\langle m|d_i|G\rangle|^2$), where, $|m\rangle$ denotes the excited state in question, $|G\rangle$, the ground state, and d_i is the ith Cartesian component of the electric dipole operator.

Peak	E (eV)	f_{12}	Polarization	Wave Function
GS[a]				$\|HF\rangle$ (0.8229)
				$\|H-3 \to L\rangle$ (0.2162)
				$\|H \to L\rangle$ (0.2072)
				$\|H-3 \to H\rangle$ (0.1544)
I	0.797	0.0119	$\perp$	$\|H-1 \to H\rangle$ (0.7357)
				$\|H-1 \to L\rangle$ (0.4693)
				$\|H-1 \to L+8\rangle$ (0.1142)
II	1.710	0.0035	$\parallel$	$\|H \to L+1\rangle$ (0.4816)
				$\|H-2 \to H\rangle$ (0.4315)
				$\|H-2 \to L\rangle$ (0.3757)
				$\|H-3 \to L+1\rangle$ (0.3709)
		0.0037	$\parallel$	$\|H \to L\rangle$ (0.5041)
				$\|H-3 \to H\rangle$ (0.4703)
III	2.840	0.0679	$\parallel$	$\|H-2 \to H\rangle$ (0.5374)
				$\|H \to L+1\rangle$ (0.5199)
				$\|H-2 \to L\rangle$ (0.3306)
				$\|H-3 \to L+1\rangle$ (0.2216)
	2.872	0.0622	$\parallel$	$\|H \to L\rangle$ (0.4906)
				$\|H-3 \to L\rangle$ (0.4499)
IV	5.710	0.0428	$\parallel$	$\|H-2 \to L\rangle$ (0.4114)
				$\|H-2 \to H\rangle$ (0.3474)
	5.730	0.0269	$\parallel$	$\|H-3 \to L\rangle$ (0.4202)
				$\|H-2 \to H; H-3 \to L\rangle$ (0.2050)
V	5.988	0.0663	$\parallel$	$\|H-3 \to L+1\rangle$ (0.3968)
				$\|H-2 \to L\rangle$ (0.3057)
				$\|H-2 \to H\rangle$ (0.1578)
	6.02	0.1270	$\parallel$	$\|H-3 \to L\rangle$ (0.2578)
				$\|H \to L\rangle$ (0.1908)
VI	7.657	0.2151	$\parallel$	$\|H \to L+2\rangle$ (0.5863)
				$\|H-3 \to L+2\rangle$ (0.2497)
				$\|H \to L+14\rangle$ (0.2431)
				$\|H \to L+4\rangle$ (0.2093)
	7.697	0.1409	$\parallel$	$\|H \to L+3\rangle$ (0.2991)
				$\|H-3 \to L+1\rangle$ (0.2648)
				$\|H-2 \to H\rangle$ (0.1794)
				$\|H-2 \to L\rangle$ (0.1521)
VII	7.893	0.2797	$\perp$	$\|H \to L+5\rangle$ (0.7611)
				$\|H-3 \to L+4\rangle$ (0.3477)

[a]GS does not correspond to any peak, instead it corresponds to the ground state wavefunction of the isomer.

Note: The polarization $\parallel$ corresponds to the absorption due to light polarized in the plane of isomer, while $\perp$ corresponds to the polarization perpendicular to that plane. In the wave function, the bracketed numbers are the CI coefficients of a given electronic configuration. Symbol L and H denote LUMO and SOMO orbitals discussed earlier. HF denotes the Hartree-Fock configuration.

Table A3.   Excitation energies, E, and many-particle wave functions of excited states corresponding to the peaks in the linear absorption spectrum of linear B_3 (*cf.* Fig. 6), along with oscillator strength of transition ($f_{12} = \frac{2\,m_e}{3\,\hbar^2}(E_2 - E_1)\sum_i |\langle m|d_i|G\rangle|^2$), where, $|m\rangle$ denotes the excited state in question, $|G\rangle$, the ground state, and d_i is the ith Cartesian component of the electric dipole operator.

Peak	E (eV)	f_{12}	Polarization	Wave Function
GS[a]				$|HF\rangle$ (0.6650)
				$|H-1 \rightarrow L; H-1 \rightarrow L\rangle$ (0.3286)
				$|H-1 \rightarrow L; H-1 \rightarrow L\rangle$ (0.3277)
				$|H \rightarrow L; H-1 \rightarrow L+1\rangle$ (0.2158)
				$|H \rightarrow L; H-1 \rightarrow L+1\rangle$ (0.2157)
I	0.723	0.0199	longitudinal	$|H \rightarrow L\rangle$ (0.8222)
II	2.707	0.0175	transverse	$|H-1 \rightarrow L\rangle$ (0.5360)
III	4.338	0.5930	longitudinal	$|H-1 \rightarrow L; H-1 \rightarrow H\rangle$ (0.5826)
				$|H-1 \rightarrow L; H-1 \rightarrow H\rangle$ (0.5826)
IV	5.937	0.0301	longitudinal	$|H-2 \rightarrow L\rangle$ (0.2497)
V	7.359	1.1053	longitudinal	$|H-1 \rightarrow L+1\rangle$ (0.3683)
				$|H-1 \rightarrow L+1\rangle$ (0.3683)
				$|H-3 \rightarrow L; H \rightarrow L\rangle$ (0.3301)
				$|H-3 \rightarrow H\rangle$ (0.2364)
VI	7.731	0.3921	longitudinal	$|H-2 \rightarrow L\rangle$ (0.3858)
				$|H \rightarrow L; H-1 \rightarrow L+4\rangle$ (0.2851)
				$|H \rightarrow L; H-1 \rightarrow L+4\rangle$ (0.2851)
	7.786	0.3062	transverse	$|H-1 \rightarrow L; H-1 \rightarrow L+4\rangle$ (0.6438)
				$|H-1 \rightarrow L; H-1 \rightarrow L+4\rangle$ (0.3905)

[a]GS does not correspond to any peak, instead it corresponds to the ground state wavefunction of the isomer.

Note: Longitudinal and transverse polarization corresponds to the absorption due to light polarized along and perpendicular to the molecular axis respectively. In the wave function, the bracketed numbers are the CI coefficients of a given electronic configuration. Symbols H and L denote HOMO and LUMO orbitals respectively, and H_1 denotes SOMOs discussed earlier. HF denotes the Hartree−Fock configuration.

Table A4. Excitation energies, E, and many-particle wave functions of excited states corresponding to the peaks in the linear absorption spectrum of rhombus B_4 (*cf.* Fig. 8), along with oscillator strength of transition ($f_{12} = \frac{2}{3}\frac{m_e}{\hbar^2}(E_2 - E_1)\sum_i |\langle m|d_i|G\rangle|^2$), where, $|m\rangle$ denotes the excited state in question, $|G\rangle$, the ground state, and d_i is the ith Cartesian component of the electric dipole operator.

Peak	E (eV)	f_{12}	Polarization	Wave Function
GS[a]				$|HF\rangle$ (0.8787)
				$|H \rightarrow L; H \rightarrow L\rangle$ (0.1147)
I	4.159	0.4684	in-plane	$|H \rightarrow L + 2\rangle$ (0.6566)
				$|H \rightarrow L + 10\rangle$ (0.3210)
				$|H - 1 \rightarrow L + 6\rangle$ (0.2773)
				$|H - 1 \rightarrow L + 17\rangle$ (0.1850)
II	6.118	0.3925	in-plane	$|H - 1 \rightarrow L + 6\rangle$ (0.5786)
				$|H - 1 \rightarrow L + 17\rangle$ (0.3285)
				$|H - 3 \rightarrow L\rangle$ (0.2656)
				$|H - 2 \rightarrow L + 11\rangle$ (0.2544)
				$|H - 2 \rightarrow L + 18\rangle$ (0.2492)
III	6.639	0.0490	in-plane	$|H - 1 \rightarrow L + 3\rangle$ (0.4496)
				$|H - 1 \rightarrow L + 13\rangle$ (0.4485)
				$|H - 4 \rightarrow L\rangle$ (0.4052)
				$|H \rightarrow L + 11\rangle$ (0.2766)
				$|H \rightarrow L + 1\rangle$ (0.2329)
				$|H \rightarrow L + 18\rangle$ (0.1905)
IV	7.311	0.2528	in-plane	$|H \rightarrow L + 2\rangle$ (0.3055)
				$|H - 2 \rightarrow L + 11\rangle$ (0.2892)
				$|H - 3 \rightarrow L\rangle$ (0.2834)
				$|H - 2 \rightarrow L + 18\rangle$ (0.2487)
				$|H - 2 \rightarrow L + 1\rangle$ (0.2029)
				$|H - 2 \rightarrow L + 5\rangle$ (0.1509)
V	7.842	0.3951	in-plane	$|H \rightarrow L + 2\rangle$ (0.4233)
				$|H \rightarrow L + 10\rangle$ (0.3270)
				$|H - 2 \rightarrow L + 11\rangle$ (0.2049)
				$|H \rightarrow L + 20\rangle$ (0.1946)
				$|H - 2 \rightarrow L + 1\rangle$ (0.1594)
				$|H - 2 \rightarrow L + 18\rangle$ (0.1582)

[a]GS does not correspond to any peak, instead it corresponds to the ground state wavefunction of the isomer.

Note: The polarization *in-plane* corresponds to the absorption due to light polarized in the plane of isomer. In the wave function, the bracketed numbers are the CI coefficients of a given electronic configuration. Symbols H/L denote HOMO/LUMO orbitals. HF denotes the Hartree-Fock configuration.

Table A5.   Excitation energies, E, and many-particle wave functions of excited states corresponding to the peaks in the linear absorption spectrum of square B_4 (*cf.* Fig. 9), along with oscillator strength of transition ($f_{12} = \frac{2}{3}\frac{m_e}{\hbar^2}(E_2 - E_1)\sum_i |\langle m|d_i|G\rangle|^2$), where, $|m\rangle$ denotes the excited state in question, $|G\rangle$, the ground state, and d_i is the ith Cartesian component of the electric dipole operator.

Peak	E (eV)	f_{12}	Polarization	Wave Function
GS[a]				$|HF\rangle$ (0.8682)
				$|H \to L; H \to L\rangle$ (0.1765)
				$|H - 2 \to L; H - 2 \to L\rangle$ (0.0920)
I	4.879	0.5678	in-plane	$|H \to L; H \to L + 1\rangle$ (0.2946)
				$|H \to L; H - 3 \to L\rangle$ (0.1909)
				$|H - 2 \to L; H - 3 \to L\rangle$ (0.1651)
II	5.462	0.0235	in-plane	$|H \to L; H \to L + 1\rangle$ (0.5893)
				$|H \to L; H \to L + 6\rangle$ (0.2477)
III	6.418	0.2842	in-plane	$|H \to L; H - 3 \to L\rangle$ (0.5379)
				$|H \to L; H \to L + 1\rangle$ (0.2922)
				$|H - 2 \to L; H - 3 \to L\rangle$ (0.1744)
IV	7.890	1.3888	in-plane	$|H \to L + 1; H - 1 \to L\rangle$ (0.2351)

[a]GS does not correspond to any peak, instead it corresponds to the ground state wavefunction of the isomer. *Note*: The polarization *in-plane* corresponds to the absorption due to light polarized in the plane of isomer. In the wave function, the bracketed numbers are the CI coefficients of a given electronic configuration. Symbols H/L denote HOMO/LUMO orbitals. HF denotes the Hartree−Fock configuration.

Table A6.   Excitation energies, E, and many-particle wave functions of excited states corresponding to the peaks in the linear absorption spectrum of linear B_4 (*cf.* Fig. 10), along with oscillator strength of transition ($f_{12} = \frac{2}{3}\frac{m_e}{\hbar^2}(E_2 - E_1)\sum_i |\langle m|d_i|G\rangle|^2$), where, $|m\rangle$ denotes the excited state in question, $|G\rangle$, the ground state, and d_i is the ith Cartesian component of the electric dipole operator.

Peak	E (eV)	f_{12}	Polarization	Wave Function
GS[a]				$|HF\rangle$ (0.5636)
				$|H \to L\rangle$ (0.4737)
				$|H - 1 \to L; H \to L + 1\rangle$ (0.2291)
				$|H - 1 \to L; H \to L + 1\rangle$ (0.2289)
I	5.363	0.0976	longitudinal	$|H \to L; H - 1 \to L + 9\rangle$ (0.3005)
				$|H \to L; H - 1 \to L + 9\rangle$ (0.3005)
				$|H \to L; H - 1 \to L + 8\rangle$ (0.2702)
				$|H \to L; H - 1 \to L + 8\rangle$ (0.2702)
				$|H \to L; H - 1 \to L + 4\rangle$ (0.2439)
				$|H \to L; H - 1 \to L + 4\rangle$ (0.2439)
II	5.947	4.1752	longitudinal	$|H - 1 \to L + 1\rangle$ (0.2957)
				$|H - 1 \to L + 1\rangle$ (0.2957)
III	7.352	1.8444	longitudinal	$|H \to L; H - 2 \to L\rangle$ (0.6477)
				$|H - 3 \to L\rangle$ (0.2966)
				$|H - 1 \to L + 1\rangle$ (0.2091)
				$|H - 1 \to L + 1\rangle$ (0.2091)
	7.380	1.0202	transverse	$|H - 1 \to L + 13\rangle$ (0.5253)

[a]GS does not correspond to any peak, instead it corresponds to the ground state wavefunction of the isomer. *Note*: Longitudinal and transverse polarization corresponds to the absorption due to light polarized along and perpendicular to the molecular axis respectively. In the wave function, the bracketed numbers are the CI coefficients of a given electronic configuration. Symbols H/L denote HOMO/LUMO orbitals. HF denotes the Hartree−Fock configuration.

Table A7. Excitation energies, E, and many-particle wave functions of excited states corresponding to the peaks in the linear absorption spectrum of distorted tetrahedron B_4 (*cf.* Fig. 11), along with oscillator strength of transition ($f_{12} = \frac{2}{3}\frac{m_e}{\hbar^2}(E_2 - E_1) \sum_i |\langle m|d_i|G\rangle|^2$), where, $|m\rangle$ denotes the excited state in question, $|G\rangle$, the ground state, and d_i is the ith Cartesian component of the electric dipole operator.

Peak	E (eV)	f_{12}	Polarization	Wave Function
GS[a]				$|HF\rangle$ (0.6493)
				$|H \to L; H \to L+2\rangle$ (0.4695)
				$|H \to L; H-3 \to L+2\rangle$ (0.1547)
I	1.000	0.0068	x	$|H \to L\rangle$ (0.8127)
				$|H \to L; H-1 \to L+2\rangle$ (0.2364)
	1.111	0.0094	y	$|H \to L+2; H \to L+1\rangle$ (0.5944)
				$|H \to L; H \to L+1\rangle$ (0.5121)
II	3.609	0.0364	x	$|H \to L; H-1 \to L+2\rangle$ (0.5094)
				$|H \to L; H-1 \to L\rangle$ (0.4535)
				$|H \to L+2\rangle$ (0.3480)
	3.754	0.0519	y	$|H \to L+1; H \to L+2\rangle$ (0.2391)
III	4.48	0.0632	z	$|H-1 \to L\rangle$ (0.4418)
IV	4.96	0.0767	z	$|H-1 \to L\rangle$ (0.2678)
				$|H \to L; H-3 \to L\rangle$ (0.2227)
V	5.92	0.0913	x	$|H-3 \to L\rangle$ (0.2191)
				$|H \to L+2; H-4 \to L\rangle$ (0.2191)
VI	6.15	0.0895	y	$|H \to L; H-3 \to L+1\rangle$ (0.2526)
VII	6.508	0.0159	z	$|H-1 \to L+2\rangle$ (0.7131)
				$|H-1 \to L\rangle$ (0.2104)
				$|H \to L+2; H \to L+2\rangle$ (0.2030)
VIII	6.858	0.1881	x	$|H \to L; H \to L+10\rangle$ (0.6912)
				$|H \to L+2; H \to L+10\rangle$ (0.3415)
				$|H \to L+18; H \to L\rangle$ (0.2759)
	6.99	0.1488	y	$|H \to L; H \to L+5\rangle$ (0.4169)
				$|H \to L+2; H \to L+5\rangle$ (0.3770)
				$|H \to L+3; H-1 \to L\rangle$ (0.2403)
				$|H-1 \to L+1\rangle$ (0.2156)
IX	7.80	0.0686	z	$|H-1 \to L; H-1 \to L+2\rangle$ (0.3386)
				$|H \to L; H-4 \to L+2\rangle$ (0.3164)
				$|H \to L; H-4 \to L+2\rangle$ (0.2987)
				$|H-1 \to L; H-1 \to L\rangle$ (0.2722)
				$|H \to L+1; H-1 \to L+3\rangle$ (0.2174)

[a]GS does not correspond to any peak, instead it corresponds to the ground state wavefunction of the isomer.

Note: The polarization x, y and z corresponds to the absorption due to light polarized along x-, y- and z-axis, respectively. In the wave function, the bracketed numbers are the CI coefficients of a given electronic configuration. Symbols H/L denote HOMO/LUMO orbitals. HF denotes the Hartree−Fock configuration.

Table A8. Excitation energies, E, and many-particle wave functions of excited states corresponding to the peaks in the linear absorption spectrum of pentagon B_5 (*cf.* Fig. 12), along with oscillator strength of transition ($f_{12} = \frac{2}{3}\frac{m_e}{\hbar^2}(E_2 - E_1)\sum_i |\langle m|d_i|G\rangle|^2$), where, $|m\rangle$ denotes the excited state in question, $|G\rangle$, the ground state, and d_i is the ith Cartesian component of the electric dipole operator.

Peak	E (eV)	f_{12}	Polarization	Wave Function
GS[a]				$\vert HF\rangle$ (0.8541) $\vert H-1 \to L\rangle$ (0.1906)
I	1.394	0.0237	$\perp$ to the plane	$\vert H \to L+1\rangle$ (0.8536) $\vert H \to L+11\rangle$ (0.1779)
II	1.818	0.0096	in-plane	$\vert H \to L\rangle$ (0.6524) $\vert H-1 \to H\rangle$ (0.4900) $\vert H \to L+3\rangle$ (0.2218)
III	3.504	0.0848	in-plane	$\vert H-2 \to L+1\rangle$ (0.5804) $\vert H-1 \to H\rangle$ (0.5131) $\vert H \to L\rangle$ (0.3441)
IV	3.868	0.0372	in-plane	$\vert H-2 \to L+1\rangle$ (0.7968) $\vert H-1 \to H\rangle$ (0.3416)
V	4.379	0.0247	in-plane	$\vert H-3 \to H\rangle$ (0.8185) $\vert H-4 \to L\rangle$ (0.1900)
VI	5.378	0.1642	in-plane	$\vert H-1 \to L\rangle$ (0.7309) $\vert H-4 \to L\rangle$ (0.3583) $\vert H-1 \to L+3\rangle$ (0.1994) $\vert H-3 \to H\rangle$ (0.1808)
	5.576	0.6640	in-plane	$\vert H-2 \to L+1\rangle$ (0.4415) $\vert H-3 \to L\rangle$ (0.4045) $\vert H-4 \to H\rangle$ (0.4000) $\vert H \to L\rangle$ (0.2399) $\vert H-1 \to L+4\rangle$ (0.2039)
VII	6.305	0.6453	in-plane	$\vert H-3 \to L\rangle$ (0.4073) $\vert H-1 \to L+4\rangle$ (0.3328) $\vert H-1 \to L+9\rangle$ (0.2952) $\vert H-2 \to L+1\rangle$ (0.2870) $\vert H-4 \to L+4\rangle$ (0.2772) $\vert H-4 \to L+9\rangle$ (0.2531)
	6.528	0.1049	in-plane	$\vert H-1 \to L\rangle$ (0.5596) $\vert H-4 \to L\rangle$ (0.3400) $\vert H-2 \to L+2\rangle$ (0.2761) $\vert H-3 \to L+4\rangle$ (0.2667) $\vert H-3 \to L+9\rangle$ (0.2598)
VIII	7.161	0.2561	in-plane	$\vert H-4 \to L+4\rangle$ (0.4305) $\vert H-4 \to L+9\rangle$ (0.3859) $\vert H-3 \to L\rangle$ (0.3776) $\vert H-1 \to L+4\rangle$ (0.2487)
	7.283	0.0781	in-plane	$\vert H \to L+6\rangle$ (0.7102) $\vert H \to L+9\rangle$ (0.3359) $\vert H-3 \to L+4\rangle$ (0.2091) $\vert H-3 \to L+9\rangle$ (0.1854)

Table A8. (*Continued*)

Peak	E (eV)	f_{12}	Polarization	Wave Function
IX	7.702	0.1345	$\perp$ to the plane	$\lvert H \to L+11\rangle$ (0.7980) $\lvert H \to L+14\rangle$ (0.2692)
	7.750	0.1150	in-plane	$\lvert H-1 \to L+3\rangle$ (0.8332) $\lvert H-1 \to L+19\rangle$ (0.1555)

[a]GS does not correspond to any peak, instead it corresponds to the ground state wavefunction of the isomer. *Note*: The polarization *in-plane* corresponds to the absorption due to light polarized in the plane of isomer. In the wave function, the bracketed numbers are the CI coefficients of a given electronic configuration. Symbols H and L denote HOMO and LUMO orbitals respectively. HF denotes the Hartree-Fock configuration.

Table A9. Excitation energies, E, and many-particle wave functions of excited states corresponding to the peaks in the linear absorption spectrum of distorted triangular-bipyramid B_5 (*cf.* Fig. 13), along with oscillator strength of transition ($f_{12} = \frac{2m_e}{3\hbar^2}(E_2 - E_1)\sum_i |\langle m|d_i|G\rangle|^2$), where, $|m\rangle$ denotes the excited state in question, $|G\rangle$, the ground state, and d_i is the ith Cartesian component of the electric dipole operator.

Peak	E (eV)	f_{12}	Polarization	Wave Function
GS[a]				$\lvert\text{HF}\rangle$ (0.8615) $\lvert H-1 \to H\rangle$ (0.2165) $\lvert H-1 \to H; H-1 \to L\rangle$ (0.1371) $\lvert H-2 \to H; H-1 \to L\rangle$ (0.1143)
I	1.774	0.0548	z	$\lvert H-1 \to L+4\rangle$ (0.8689)
II	3.161	0.0763	y	$\lvert H-2 \to H\rangle$ (0.8734) $\lvert H-1 \to H; H-1 \to L\rangle$ (0.2303)
III	4.274	0.0509	z	$\lvert H-1 \to L+2\rangle$ (0.8666) $\lvert H-1 \to L+6\rangle$ (0.1775)
IV	5.487	0.1949	y	$\lvert H-1 \to H; H-1 \to L\rangle$ (0.7812) $\lvert H-2 \to H\rangle$ (0.2336) $\lvert H-2 \to H; H-1 \to L\rangle$ (0.2332)
V	6.408	0.1170	z	$\lvert H-4 \to H\rangle$ (0.7837) $\lvert H-2 \to L+2\rangle$ (0.3357) $\lvert H-2 \to H; H-1 \to L+1\rangle$ (0.2274)
VI	7.519	0.4523	x	$\lvert H-2 \to H; H-1 \to L+2\rangle$ (0.8133) $\lvert H-2 \to H; H-1 \to L+6\rangle$ (0.2669)
VII	7.744	0.0177	x	$\lvert H-1 \to L; H-1 \to L+1\rangle$ (0.6105) $\lvert H-1 \to L+4\rangle$ (0.4305) $\lvert H-2 \to L+1\rangle$ (0.2271)

[a]GS does not correspond to any peak, instead it corresponds to the ground state wavefunction of the isomer.
Note: The polarization x, y and z corresponds to the absorption due to light polarized along x-, y- and z-axis, respectively. In the wave function, the bracketed numbers are the CI coefficients of a given electronic configuration. Symbols H and L denote HOMO and LUMO orbitals respectively. HF denotes the Hartree−Fock configuration.

References

1. J. A. Alonso, *Structure and Properties of Atomic Nanostructures* (Imperial College Press, London, 2005).
2. T. Kondow, Y. Kawazoe and K. Ohno, *Clusters and Nanomaterials* (Springer-Verlag, Berlin, 2002).
3. J. Jellinek, *Theory of Atomic and Molecular Clusters — With a Glimpse at Experiments* (Springer-Verlag, Berlin, 1999).
4. W. A. de Heer, *Rev. Mod. Phys.* **65**, 611 (1993).
5. J. Plešek, *Chem. Rev.* **92**, 269 (1992).
6. R. H. Xie, G. W. Bryant, J. Zhao, T. Kar and V. H. Smith, *Phys. Rev. B* **71**, 125422 (2005).
7. N. S. Goroff, *Acc. Chem. Res.* **29**, 77 (1996).
8. T. Belz, F. Z. H. Werner, M. W. U. Klengler, E. Z. B. Tesche, A. Reller and R. Schlögl, *Angew. Chem. Int. Ed.* **33**, 1866 (2003).
9. R. N. Grimes, *J. Chem. Educ.* **81**, 657 (2004).
10. Y. Zhao, Y. H. Kim, A. C. Dillon, M. J. Heben and S. B. Zhang, *Phys. Rev. Lett.* **94**, 155504 (2005).
11. I. Cabria, M. J. López and J. A. Alonso, *Nanotechnology* **17**, 778 (2006).
12. S. A. Shevlin and Z. X. Guo, *Phys. Rev. B* **76**, 024104 (2007).
13. S. Sahu and A. Shukla, *Nano. Res. Lett.* **5**, 714 (2010).
14. H. J. Zhai, B. Kiran, J. Li and L. S. Wang, *Nat. Mater.* **2**, 827 (2003).
15. L. Hanley, J. L. Whitten and S. L. Anderson, *J. Phys. Chem.* **92**, 5803 (1988).
16. H. J. Zhai, A. N. Alexandrova, K. A. Birch, A. I. Boldyrev and L. S. Wang, *Angew. Chem. Int. Ed.* **42**, 6004 (2003).
17. C. Romanescu, T. R. Galeev, W. L. Li, A. I. Boldyrev and L. S. Wang, *Angew. Chem. Int. Ed.* **50**, 9334 (2011).
18. B. Kiran, S. Bulusu, H. J. Zhai, S. Yoo, X. C. Zeng and L. S. Wang *Proc. Nat. Acad. Sci. USA* **102**, 961 (2005).
19. S. J. La Placa, P. A. Roland and J. J. Wynne, *Chem. Phys. Lett.* **190**, 163 (1992).
20. J. S. Lauret, R. Arenal, F. Ducastelle, A. Loiseau, M. Cau, B. Attal-Tretout, E. Rosencher and L. Goux-Capes, *Phys. Rev. Lett.* **94**, 037405 (2005).
21. N. G. Szwacki, A. Sadrzadeh and B. I. Yakobson, *Phys. Rev. Lett.* **98**, 166804 (2007).
22. S. Chacko, D. G. Kanhere and I. Boustani, *Phys. Rev. B* **68**, 035414 (2003).
23. A. Abdurahman, A. Shukla and G. Seifert, *Phys. Rev. B* **66**, 155423 (2002).
24. M. P. Johansson, *J. Phys. Chem. C* **113**, 524 (2009).
25. D. E. Bean and P. W. Fowler, *J. Phys. Chem. C* **113**, 15569 (2009).
26. S. R. Langhoff and C. W. Bauschlicher, *J. Chem. Phys.* **95**, 5882 (1991).
27. P. J. Bruna and J. S. Wright, *J. Chem. Phys.* **91**, 1126 (1989).
28. I. A. Howard and A. K. Ray, *Z. Phy. D.* **42**, 299 (1997).
29. I. Boustani, *Phys. Rev. B* **55**, 16426 (1997).
30. J. Niu, B. K. Rao and P. Jena, *J. Chem. Phys.* **107**, 132 (1997).
31. M. Atiş, C. Özdogan and Z. B. Güvenç, *Int. J. Quantum Chem.* **107**, 729 (2007).
32. J. I. Aihara, H. Kanno and T. Ishida, *J. Am. Chem. Soc.* **127**, 13324 (2005).
33. M. Saito and Y. Miyamoto, *Phys. Rev. Lett.* **87**, 035503 (2001).
34. C. R. C. Wang, S. Pollack, D. Cameron and M. M. Kappes, *J. Chem. Phys.* **93**, 3787 (1990).
35. J. Bowlan, A. Liang and W. A. de Heer, *Phys. Rev. Lett.* **106**, 043401 (2011).
36. G. Pal, Y. Pavlyukh, W. Hübner and H. C. Schneider, *Eur. Phys. J. B* **79**, 327 (2011).
37. I. Boustani, W. Pewestorf, P. Fantucci, V. B. Koutecký and J. Koutecký, *Phys. Rev. B* **35**, 9437 (1987).
38. J. M. Pacheco and J. L. Martins, *J. Chem. Phys.* **106**, 6039 (1997).
39. M. A. L. Marques and S. Botti, *J. Chem. Phys.* **123**, 014310 (2005).
40. S. Botti, A. Castro, N. N. Lathiotakis, X. Andrade and M. A. L. Marques, *Phys. Chem. Chem. Phys.* **11**, 4523 (2009).
41. M. W. Schmidt, K. K. Baldridge, J. A. Boatz, S. T. Elbert, M. S. Gordon, J. H. Jensen, S. Koseki, N. Matsunaga, K. A. Nguyen, S. Su, T. L. Windus, M. Dupuis and J. A. Montgomery. *J. Comput. Chem.* **14**, 1347 (1993).
42. L. E. McMurchie, S. T. Elbert, S. R. Langhoff and E. R. Davidson, *MELD Package from Indiana University. It has been Modified by us to Handle Bigger Systems.*
43. P. Sony and A. Shukla, *J. Chem. Phys.* **131**, 014302 (2009).
44. P. Sony and A. Shukla, *Phys. Rev. B* **75**, 155208 (2007).
45. P. Sony and A. Shukla, *Phys. Rev. B* **71**, 165204 (2005).
46. A. Shukla, *Phys. Rev. B* **65**, 125204 (2002).
47. K. L. Schuchardt, B. T. Didier, T. Elsethagen, L. Sun, V. Gurumoorthi, J. Chase, J. Li and T. L. Windus, *J. Chem. Inf. Model* **47**, 1045 (2007).
48. D. Feller, *J. Comput. Chem.* **17**, 1571 (1996).
49. J. Blanc, V. B. Koutecký, M. Broyer, J. Chevaleyre, P. Dugourd, J. Koutecký, C. Scheuch, J. P. Wolf and L. Wöste, *J. Chem. Phys.* **96**, 1793 (1992).
50. K. P. Huber and G. Herzberg, *Molecular Spectra and Molecular Structure: (IV). Constants of Diatomic Molecules* (Van Nostrand, Reinhold, New York, 1979).